



**HAL**  
open science

## Controlled hydrophobic modification of cellulose nanocrystals for tunable Pickering emulsions

William Dufefoi, Benjamin Dhuiège, Isabelle Capron, Gilles Sèbe

### ► To cite this version:

William Dufefoi, Benjamin Dhuiège, Isabelle Capron, Gilles Sèbe. Controlled hydrophobic modification of cellulose nanocrystals for tunable Pickering emulsions. *Carbohydrate Polymer Technologies and Applications*, 2022, 3, pp.100210. 10.1016/j.carpta.2022.100210 . hal-03695031

**HAL Id: hal-03695031**

**<https://hal.inrae.fr/hal-03695031v1>**

Submitted on 23 Aug 2023

**HAL** is a multi-disciplinary open access archive for the deposit and dissemination of scientific research documents, whether they are published or not. The documents may come from teaching and research institutions in France or abroad, or from public or private research centers.

L'archive ouverte pluridisciplinaire **HAL**, est destinée au dépôt et à la diffusion de documents scientifiques de niveau recherche, publiés ou non, émanant des établissements d'enseignement et de recherche français ou étrangers, des laboratoires publics ou privés.



Distributed under a Creative Commons Attribution - NonCommercial - NoDerivatives 4.0 International License

1

## 2 **Controlled hydrophobic modification of cellulose nanocrystals for tunable**

### 3 **Pickering emulsions**

4 William Dufouir<sup>b</sup>, Benjamin Dhuiège<sup>a</sup>, Isabelle Capron<sup>b,\*</sup>, Gilles Sèbe<sup>a,\*</sup>

5 <sup>a</sup> Univ. Bordeaux, CNRS, Bordeaux INP, LCPO, UMR 5629, F-33600 Pessac, France

6 <sup>b</sup> INRAE, UR BIA, F-44316, Nantes, France

7

#### 8 **Abstract**

9 Cellulose nanocrystals (CNC) are known to promote highly stable oil-in-water (O/W)  
10 Pickering emulsions. Our work consisted in producing CNCs with different  
11 hydrophilic/hydrophobic balance at their surface by chemical functionalization (acylation  
12 with model functional vinyl esters) and to identify the adequate conditions allowing the  
13 stabilization of direct O/W or inverse W/O Pickering emulsions. Whatever the surface degree  
14 of substitution ( $DS_{\text{Surf}}$ ), CNCs grafted with linear acyl chains of 2 to 6 carbons led to the  
15 exclusive formation of direct O/W emulsions. Distinctively, both O/W and W/O emulsions  
16 could be obtained when the linear chain contained 8 carbons or more, at low and high  $DS_{\text{Surf}}$ ,  
17 respectively. By adjusting the length of the grafted chain,  $DS_{\text{Surf}}$  and particles concentration,  
18 we were able to monitor the type of emulsion formed, droplet size and surface coverage at the  
19 oil/water interface.

## 20 **1. Introduction**

21 An emulsion is a system of dispersed droplets of one immiscible liquid in another,  
22 stabilized by an amphiphilic surface reactive agent composed by both a polar hydrophobic  
23 and a non-polar hydrophilic extremities. Emulsions are being used in a broad range of daily  
24 life products, such as in food industry, cosmetics, or pharmaceuticals, and in most cases, the  
25 surface active agents used are surfactants; i.e. chemical products. However, surfactants may  
26 be the cause of some undesirable adverse effects, such as skin irritation for the consumer, but  
27 also have negative impact on the environment (Belanger et al., 2006). As an alternative to  
28 chemical surfactants, emulsions can also be stabilized by the use of solid particles, forming  
29 so-called Pickering emulsions (Pickering, 1907; Arditty, Whitby, Binks, Schmitt, & Leal-  
30 Calderon, 2003). This type of emulsion also has the advantage of having an adsorption energy  
31 at the interface thousands times greater than for surfactants, leading to a better stability of the  
32 emulsion with the particles irreversibly anchored at the interface of the emulsion (Binks,  
33 2002). Among the most interesting solid particles used for Pickering emulsions are cellulose  
34 nanocrystals (CNCs). Indeed, cellulose is a biodegradable biopolymer, main building block of  
35 trees and plants and composed of ordered crystalline regions interrupted by amorphous  
36 regions. The amorphous regions can be hydrolyzed using sulfuric acid, resulting in the  
37 production of rod-like nanocrystals decorated with sulfate half-ester groups at their surface  
38 (Habibi, Lucia, & Rojas, 2010; Moon, Martini, Nairn, Simonsen, & Youngblood, 2011). The  
39 use of unmodified CNCs as Pickering emulsion stabilizer has been first demonstrated in 2011  
40 (Kalashnikova, Bizot, Cathala, & Capron, 2011). It was shown that unmodified CNCs  
41 dispersed in water, mixed with an apolar phase, such as hexadecane, can adsorb at the oil-  
42 water interface, preventing destabilization from coalescence for a very long period of more  
43 than one year. Small angle neutron scattering experiments carried out with a contrast variation  
44 method probed the arrangement of CNCs at the interface. These results showed that the (200)

45 crystalline plane of the CNCs directly interacts with the interface without deforming it  
46 (Cherhal, Cousin, & Capron, 2016). As a consequence, surface interactions occur between the  
47 CH of the CNCs and the alkyl chain of hexadecane after desorption of the aqueous layer.  
48 These performances in stabilizing oil-in-water (O/W) Pickering emulsions are reached  
49 through the formation a dense 2D interfacial network around the droplets (Kalashnikova,  
50 Bizot, Cathala, & Capron, 2012), with the possibility to control their size by varying the  
51 CNCs concentration (Capron, Rojas, & Bordes, 2017; Cherhal, Cousin, & Capron, 2016).  
52 This process generally requires the addition of salt to screen the repulsion between the  
53 negatively charged particles. In another approach, surface modification can also be carried out  
54 (Eyley & Thielemans, 2014; Habibi, 2014), to finely adjust the hydrophilic/hydrophobic  
55 balance at the surface of the CNCs. In that case, O/W (Sèbe, Ham-Pichavant, & Pecastaings,  
56 2013; Werner, Schmitt, Sèbe, & Héroguez, 2017; Werner, Sèbe & Héroguez, 2018), water-in-  
57 oil (W/O) (Xhanari, Syverud, & Stenius, 2011; Lee, Blaker, Murakami, Heng, & Bismarck,  
58 2014; Zhang, Tam, Wang, & Sèbe, 2018; Werner, Schmitt, Sèbe, & Héroguez, 2019) or  
59 double (Cunha, Mougél, Cathala, Berglund, & Capron, 2014) Pickering emulsions can be  
60 obtained, depending on the surface wettability of the particles.

61 In this work, a wide range of amphiphilic cellulose nanocrystals were prepared by  
62 acylation with model vinyl esters of various chain length and surface degree of substitution  
63 ( $DS_{\text{Surf}}$ ), in order to i) investigate the impact of the surface functionalization on the properties  
64 of Pickering emulsions prepared from hexadecane, and ii) identify the adequate conditions  
65 allowing the stabilization of O/W or W/O emulsions.

## 66 2. Material and methods

### 67 2.1 Material

68 Cellulose nanocrystals (CNCs) were isolated by sulfuric acid treatment of wood pulp and  
69 purchased from the University of Maine. Vinyl esters (in brackets: nomenclature, degree of  
70 purity) were purchased from Sigma Aldrich or TCI suppliers and not further purified before  
71 use: vinyl acetate (VA, 99%, Sigma), vinyl propionate (VPro, 98%, Sigma), vinyl butyrate  
72 (VBut, 98%, TCI), vinyl hexanoate (VHex, 99%, TCI), vinyl n-octanoate (VOct, 99%, TCI),  
73 vinyl decanoate (VDec, 99%, TCI), vinyl laurate (VLau, 99%, TCI), Vinyl myristate (VMyr,  
74 99%, TCI), vinyl palmitate (VPalm, 96%, TCI) and vinyl stearate (VSte, 95%, TCI).  
75 Potassium carbonate ( $K_2CO_3$ ), dimethylsulfoxide (DMSO), tetrahydrofuran (THF), toluene,  
76 hexadecane, fluorescein, technical acetone and ethanol were purchased from Sigma Aldrich.  
77 DMSO and  $K_2CO_3$  were systematically dried beforehand: on 5-Å molecular sieve for DMSO;  
78 in an oven at 50°C for  $K_2CO_3$  (overnight).

### 79 2.2 Chemical functionalization of the CNCs

80 After weighing 2.5 g of CNCs and 1.0 g of  $K_2CO_3$  in a double-necked 150 mL flask,  
81 100 mL of dried DMSO was added and the solution was sonicated for 1 min (Bandelin, MS72  
82 probe, 1.5 kJ). The volume of vinyl ester added was calculated for each treatment, to fit the  
83 molar ratio  $N_{\text{vinyl ester}}/N_{\text{OHs}} = 3.75$ , with  $N_{\text{OHs}}$  corresponding to the number of OH groups  
84 available at the surface of the CNCs (estimated at 3.1 mmol.g<sup>-1</sup> in Brand, Pecastaings, &  
85 Sèbe, 2017). After introduction of the vinyl ester, the mixture was heated in an oil bath  
86 sustained at 80°C, and magnetically stirred at 250 rpm for 5h. The reaction medium was then  
87 sampled at different periods of time (10 min, 15 min, 30 min, 45 min, 1h, 2h, 3h, 4h or 5h).  
88 Each sample was quenched with THF, and then cooled down in a water bath until room  
89 temperature was reached. Any remaining reagent or organic by-products was removed by  
90 several successive washing/sedimentation steps using 1) THF, 2) ethanol and 3) acetone, and

91 with the help of a centrifuge. The modified particles were then dialyzed in water for two days  
92 using a 1 kDa regenerated cellulose membrane and changing the water bath two times a day,  
93 to remove the  $K_2CO_3$  catalyst. Finally, the particles were re-dispersed by sonication and  
94 freeze-dried.

### 95 2.3 Fourier Transform Infrared Spectroscopy (FT-IR)

96 1-2 wt. % of modified CNC was grinded in a KBr matrix, then pressed under 200 bars for  
97 5 min to form a pellet. The spectra were recorded on a Fourier Transform Infrared Bruker  
98 spectrometer in transmission mode. Spectra were recorded between  $4000$  and  $400\text{ cm}^{-1}$ , with a  
99 resolution of  $4\text{ cm}^{-1}$ , and using 64 scans. The spectra were assigned to the same baseline and  
100 normalized on the C-O stretching vibration of the glucopyranose ring of cellulose at  $1060\text{ cm}^{-1}$ .  
101

### 102 2.4 Solid-state $^{13}C$ CP-MAS NMR spectroscopy

103  $^{13}C$  magic angle spinning (MAS) NMR measurements were performed on a 500 MHz  
104 Bruker Avance II NMR spectrometer WB (Wissembourg, France), working at frequency of  
105  $125.8\text{ MHz}$  (4 mm dual CPMAS (1H/BB)). Samples were placed into 4 mm Zirconia rotors  
106 (Cortecnet, Paris) of various volumes (70 to  $90\text{ }\mu\text{L}$ ), closed with a Kel-F cap, then spun at the  
107 magic angle frequency set to  $10\text{ kHz}$ . All spectra were recorded using a cross polarization,  
108 CP, pulse sequence with a two-pulse phase modulation (TPPM) proton decoupling and with a  
109 recycling delay of 5 s at 298 K. An average of 2000 scans was collected for each spectrum  
110 and a Lorentzian filtering function of 3 Hz was applied.  $^{13}C$  chemical shifts are reported  
111 relative to the glycine external reference, whose carbonyl group was set at 176.03 ppm.

### 112 2.5 Elaboration of the Pickering emulsions

113 CNCs grafted with alkyl linear chains varying in lengths (from C2 to C18) and surface  
114 degree of substitution ( $DS_{\text{surf}} = 0.04$  to 0.66) were dispersed at the required concentration in

115 the continuous phase, being water or hexadecane according to the emulsion type. Two ml of  
116 the different Pickering emulsions were prepared, with a W/O ratio of 80/20 v/v for direct  
117 emulsions and 20/80 v/v for inverse emulsions. The amount of CNCs was adjusted to reach a  
118 concentration of 8 mg of modified CNC per ml of oil phase (i.e. 3.2 and 12.8 mg of CNCs for  
119 the 80/20 and 20/80 ratios, respectively). For direct emulsions, 0.4 mL of hexadecane was  
120 added to 1.6mL of aqueous suspension of modified CNCs containing 50 mM NaCl. For  
121 inverse emulsions, the modified CNCs were dispersed in hexadecane and 0.4 mL of water  
122 containing fluorescein and 50 mM NaCl was added. In both cases, the mixture was then  
123 sonicated with an ultrasonic device equipped with a dipping titanium probe (QSonica Q700,  
124 150 J by alternating 2 s sonication with a 1 s standby for a total of 60 s).

#### 125 *2.6 Determination of the emulsion type using fluorescence microscopy*

126 The emulsions were systematically visualized by transmission optical microscopy with  
127 fluorescence detection in order to determine the type of emulsion formed (direct or inverse).  
128 A total of 5  $\mu$ L of the resulting Pickering emulsion was poured onto a slide with spacer and  
129 observed with a BX51 Olympus microscope.

#### 130 *2.7 Droplet size analyses with increasing concentrations of grafted CNCs*

131 The droplet diameters distributions were measured by laser light scattering using a  
132 Horiba LA-960 particle size distribution analyzer (Kyoto, Japan) for the different modified  
133 CNCs at concentrations ranging from 0.4 to 16 mg of CNCs per ml of dispersed phase in the  
134 range 0.01–5000  $\mu$ m. An analysis model was used with refractive index of 1.43 and 1.33 for  
135 hexadecane and water, respectively. Measurements were carried out on direct emulsions only.  
136 Depending on the samples, 50 to 200  $\mu$ l of the emulsions were introduced into the cell in  
137 order to reach a transmittance around 95–97%. The alignment was performed before each  
138 measurement and data acquisition times were set as default. The measurements were  
139 systematically carried out in triplicate. The diameter was expressed as surface mean diameter

140 D(3,2) (Sauter diameter). The surface coverage (C) was determined from the ratio of  
141 theoretical maximum surface area susceptible to be covered by the particles  $S_p$ , and the total  
142 surface displayed by the radius of the oil droplets  $S_d$  (Kalashnikova, Bizot, Cathala, &  
143 Capron, 2011):

$$144 \quad C = \frac{S_p}{S_d} = \frac{m_p D}{6h\rho V_{oil}} \quad \text{Eq. 1}$$

145 where  $m_p$  is the mass of CNCs introduced per mL of the dispersed phase, D is the sauter  
146 mean diameter of the droplets (also called  $D_{3,2}$ ),  $h$  is the thickness defined by AFM,  $\rho$  is the  
147 CNCs density (1.6 g/cm<sup>3</sup>) and  $V_{oil}$  is the volume of oil included in the emulsion after  
148 centrifugation.



149 **3. Results and discussion**

150 *3.1 Chemical modification of the CNCs*

151 The cellulose nanocrystals (CNCs) used in this study were obtained by sulphuric acid  
152 hydrolysis of wood pulp. They consist of negatively charged rod-like particles (Zeta potential  
153 of  $-51 \pm 6$  mV) with dimensions of  $110 \pm 48$  nm in length and  $4.8 \pm 1.1$  nm in thickness as  
154 determined by atomic force microscopy (Brand, Pecastaings, & Sèbe, 2017; Dhuiège,  
155 Pecastaings, & Sèbe, 2019). The amount of hydroxyl groups at their surface was estimated at  
156 a value of  $3.1 \pm 0.1$  mmol.g<sup>-1</sup>, which corresponds to 16.7 % of the total number of OH groups  
157 found in the particle (Brand, Pecastaings, & Sèbe, 2017). From this material, amphiphilic  
158 CNCs were produced by substituting some of the hydrophilic surface hydroxyl groups by  
159 hydrophobic acyl moieties, through an acylation reaction based on the transesterification of  
160 vinyl esters and catalyzed by potassium carbonate (Fig. 1). During the reaction, the released  
161 vinyl alcohol tautomerizes quickly to acetaldehyde, shifting the equilibrium towards the  
162 formation of the acylated product (Brand, Pecastaings, & Sèbe, 2017). The  
163 hydrophilic/hydrophobic balance at the CNCs surface was then finely monitored by varying i)  
164 the chain length of the grafted acyl moieties (from C2 to C18) and ii) the reaction time.

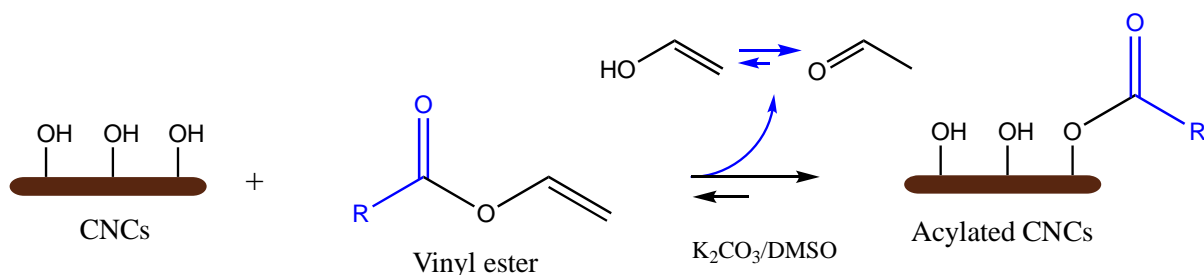
165

166

167

168

169

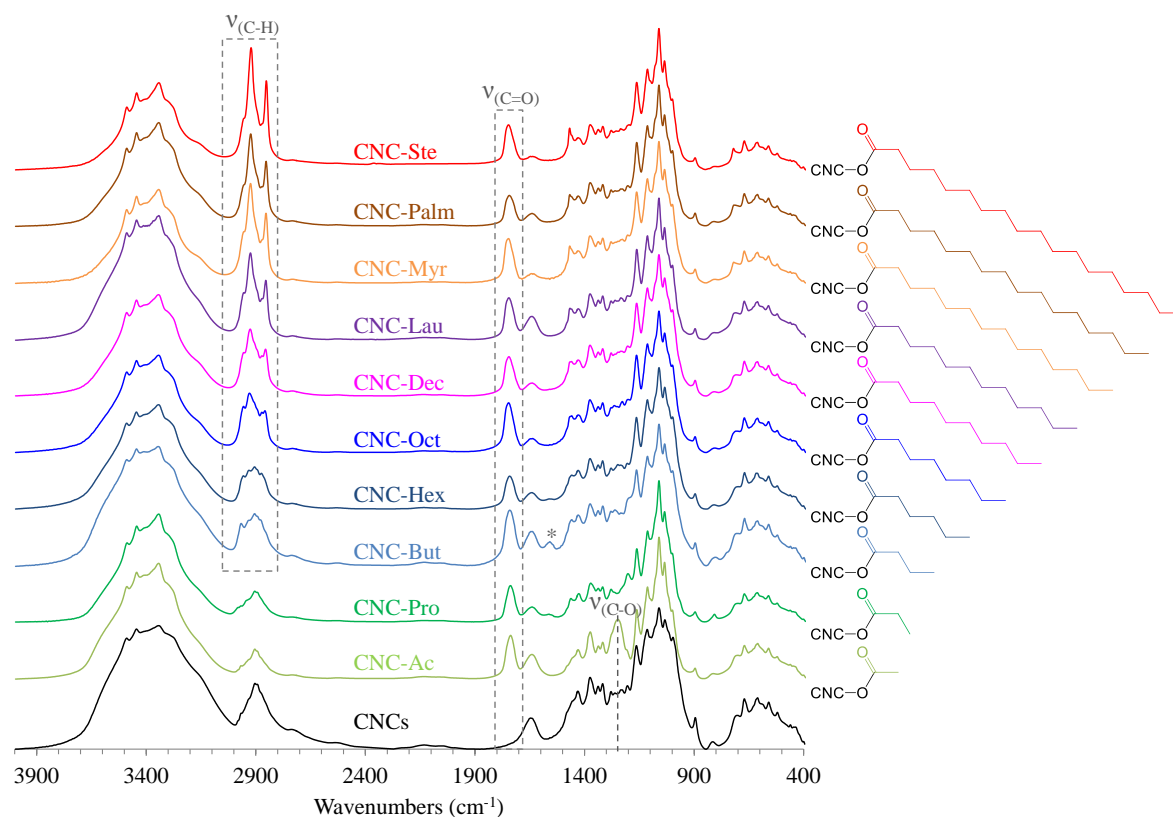


170

171 R = -CH<sub>3</sub> (CNC-Ac/C2), -CH<sub>2</sub>CH<sub>3</sub> (CNC-Pro/C3), -CH<sub>2</sub>CH<sub>2</sub>CH<sub>3</sub> (CNC-But/C4), -  
 172 CH<sub>2</sub>[CH<sub>2</sub>]<sub>3</sub>-CH<sub>3</sub> (CNC-Hex/C6), -CH<sub>2</sub>[CH<sub>2</sub>]<sub>5</sub>-CH<sub>3</sub> (CNC-Oct/C8), -CH<sub>2</sub>[CH<sub>2</sub>]<sub>7</sub>-CH<sub>3</sub> (CNC-  
 173 Dec/C10), -CH<sub>2</sub>[CH<sub>2</sub>]<sub>9</sub>-CH<sub>3</sub> (CNC-Lau/C12), -CH<sub>2</sub>[CH<sub>2</sub>]<sub>11</sub>-CH<sub>3</sub> (CNC-Myr/C14), -  
 174 CH<sub>2</sub>[CH<sub>2</sub>]<sub>13</sub>-CH<sub>3</sub> (CNC-Palm/C16), -CH<sub>2</sub>[CH<sub>2</sub>]<sub>15</sub>-CH<sub>3</sub> (CNC-Ste/C18)

175 **Fig. 1.** General scheme for the surface acylation of the CNCs with vinyl esters of various  
 176 chain lengths (in brackets: nomenclature of the sample/number of carbons in the  
 177 corresponding grafted chain).

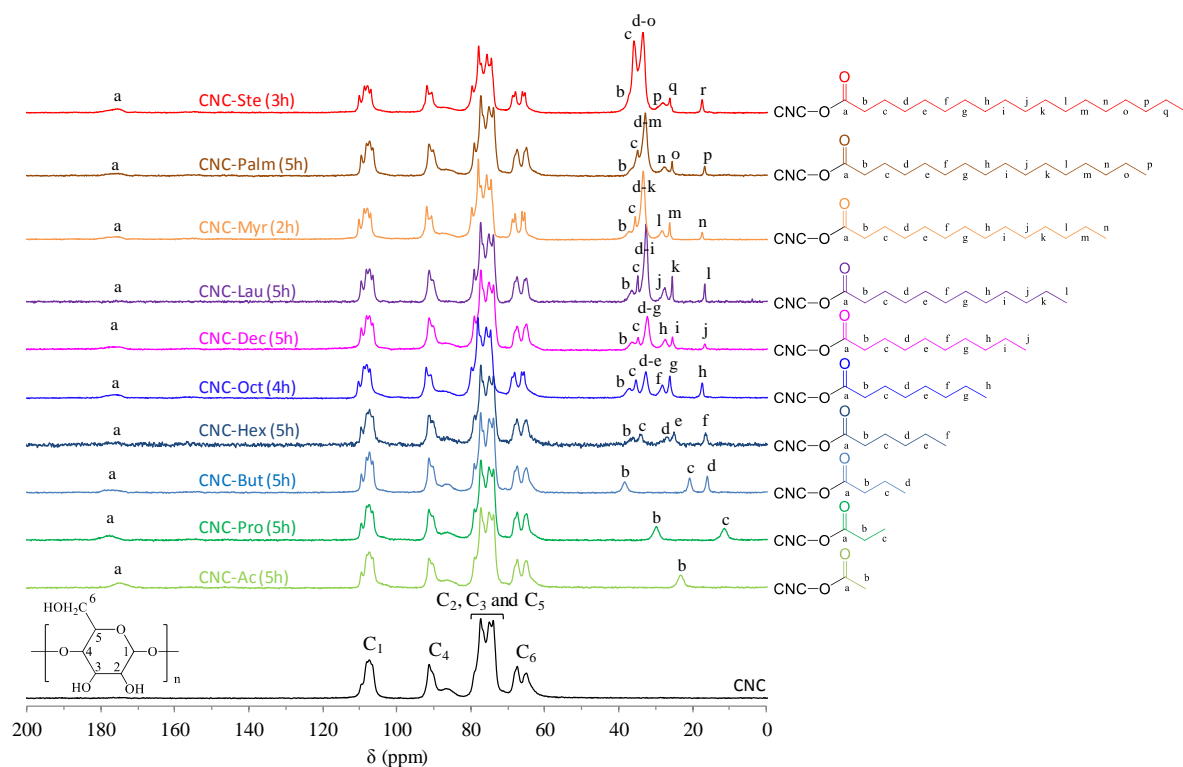
178 The efficiency of the reaction was confirmed by observing the characteristic vibrations  
 179 and chemical shifts of the grafted acyl moieties in the FT-IR and <sup>13</sup>C CP-MAS NMR spectra  
 180 of the modified material (Fig. 2 and 3, respectively). In the FT-IR spectra, the stretching  
 181 vibration of the carbonyl bond emerges at 1740 cm<sup>-1</sup> (ν<sub>C=O</sub>), while the C-H stretchings of the  
 182 CH<sub>2</sub> and -CH<sub>3</sub> groups are observed at 2925 and 2850 cm<sup>-1</sup>. The C-O stretching of the ester  
 183 bond is also observed at 1230 cm<sup>-1</sup> in the case of the acetylated sample (CNC-Ac).



184

185 **Fig. 2.** FTIR spectra of the unmodified and acylated CNCs after 5h of reaction. Traces of  
 186 remaining potassium carbonate catalyst were sometimes observed (\*).

187 In the  $^{13}\text{C}$  CP-MAS NMR spectra (Fig. 3), the carbons of cellulose resonate at 110 ppm  
 188 ( $\text{C}_1$ ), 94 ppm ( $\text{C}_4$  crystalline), 89 ppm ( $\text{C}_4$  amorphous), 77-80 ppm ( $\text{C}_2$ ,  $\text{C}_3$  and  $\text{C}_5$ ), 70 ppm  
 189 ( $\text{C}_6$  crystalline) and 68 ppm ( $\text{C}_6$  amorphous) (Attala, Gast, Sindorf, Bartuska, & Maciel,  
 190 1980), while the grafted moieties can be seen at 175 ppm (signal of the carbonyl) and in the  
 191 10-40 ppm region (signals of the methylene and methyl carbons). Whatever the sample, the  
 192 NMR cellulose pattern was not modified by the acylation treatment and the signals  
 193 corresponding to the crystalline domains retained their sharpness, which is consistent with a  
 194 grafting limited to the outer surface of the nanoparticles.



195

196 **Fig. 3.**  $^{13}\text{C}$  solid-state CP-MAS NMR spectra of the unmodified and acylated CNCs, with  
 197 the assignment of the characteristic signals (reaction time in brackets).

198 The average degree of substitution (DS) per anhydroglucose unit (AGU) was deduced  
 199 from the NMR spectra, by comparing the average integral per carbon for the grafted chain  
 200 (between 0 and 40 ppm and at 180 ppm), with the integral of the  $\text{C}_1$  carbon of cellulose used  
 201 as reference:

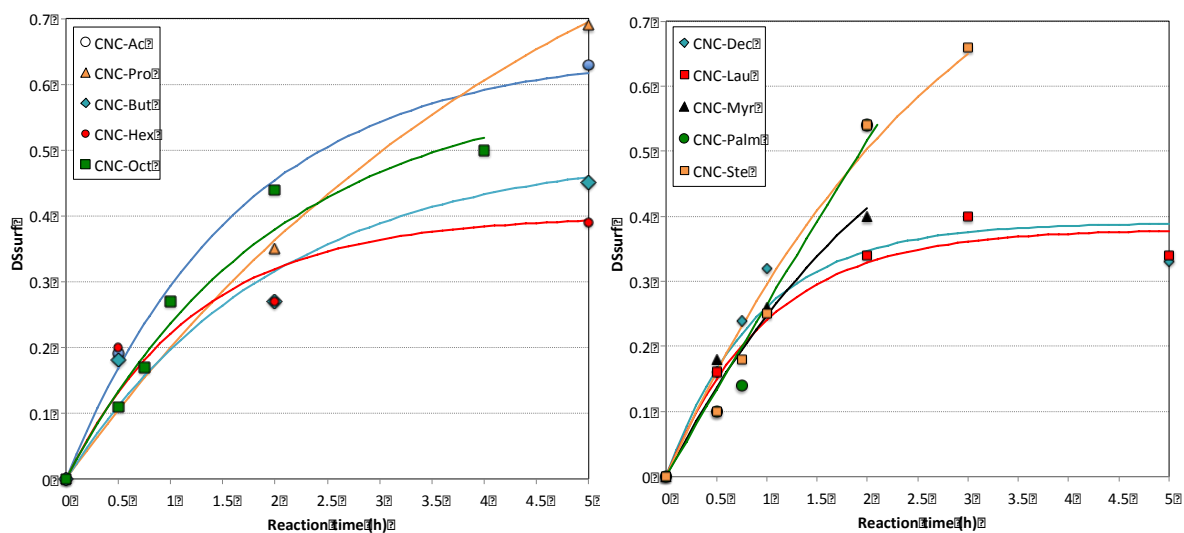
$$202 \quad \text{DS} = \frac{\text{Sum of the integrals for the grafted chain/number of carbons in the chain}}{\text{Integral of the C1 of cellulose}} \quad \text{Eq. 2}$$

203

204 This DS was later converted into a surface degree of substitution ( $\text{DS}_{\text{Surf}}$ ), knowing that only  
 205 16.7 % of the hydroxyl groups – i.e. 33.4 % of the total AGU – are located at the surface of  
 206 the CNCs and hence accessible for a chemical reaction (Brand, Pecastaings, & Sèbe, 2017):

$$207 \quad \text{DS}_{\text{Surf}} = \text{DS}/0.334. \quad \text{Eq. 3}$$

208 As only 1.5 OH per AGU (in average) is truly accessible at the surface (Eyley, &  
 209 Thielemans, 2014), the maximum value that the  $DS_{Surf}$  can reach is 1.5 (which is attained  
 210 when all the surface OH groups are substituted). The extent of surface grafting over time was  
 211 then quantified for each treatment, by plotting the  $DS_{Surf}$  as a function of reaction time  
 212 (Fig. 4).



213  
 214 **Fig. 4.** Evolution of the  $DS_{Surf}$  as a function of reaction time for the different acylated  
 215 samples.

216 The reaction kinetics were quite similar for all treatments during the first hour ( $DS_{Surf} =$   
 217 0.2-0.3 after 1 h), but discrepancies were increasingly noted as the reactions further  
 218 proceeded. In most cases, a  $DS_{Surf}$  of 0.4-0.5 was reached after 2 to 5 h of reaction, but a  
 219 number of samples displayed a higher modification rate, namely CNC-Ac, CNC-Pro, CNC-  
 220 Palm and CNC-Ste ( $DS_{Surf} = 0.5$  to 0.7). The higher reactivity of the corresponding vinyl  
 221 esters has not been explained at this stage of the study (the reactivity is obviously not simply  
 222 related to the bulkiness of the reactant). The  $O_3$  hydroxyl being involved in the strong  $O_3$ -  
 223  $H \cdots O_5$  intrachain hydrogen bond (Eyley, & Thielemans, 2014), the reactivity of the hydroxyl  
 224 groups at the cellulose surface should decrease in the order  $O_6 \geq O_2 > O_3$ , as was observed in  
 225 the case of the heterogeneous acetylation of cellulose (Goodlett, Dougherty, & Patton, 1971).

226 Due to bulkiness of most vinyl esters, it is also likely that only the O<sub>6</sub> hydroxyl is modified  
227 when the DS<sub>surf</sub> is below 0.5 (i.e. when less than one third of the surface OH groups are  
228 modified). Above this value, some O<sub>2</sub> hydroxyls should start to be acylated. In any case, the  
229 different treatments performed here allowed obtaining a wide variety of amphiphilic CNCs  
230 grafted with chains of various lengths (from C2 to C18) and various surface degree of  
231 substitution (DS<sub>surf</sub> = 0.1 to 0.7), which were used as model Pickering particles in subsequent  
232 investigations.

### 233 *3.2 Impact of grafting on direct O/W emulsions*

234 In a first set of experiments, various emulsions were prepared by sonicating the CNCs  
235 aqueous suspensions with hexadecane, at a W/O volume ratio of 80/20, and observed after  
236 24h. The type of emulsion (O/W or W/O) was inferred by pouring a drop of emulsion in a  
237 volume of either hexadecane or water (Fig S1 in Supplementary Material). In these  
238 conditions, stable O/W emulsions were systematically obtained with the particles grafted with  
239 short acyl chains (C2 to C6), regardless of the DS<sub>surf</sub>. For chains with more than 8 carbons,  
240 dense and resistant O/W emulsions could be produced only when the DS<sub>surf</sub> was  $\leq 0.15$ , the  
241 emulsions being unstable at higher DS<sub>surf</sub> (Fig. 5). This behavior is directly linked to the high  
242 hydrophobicity of the acyl groups of 8 carbons or more, which confer an excessive  
243 hydrophobicity to the particles when DS<sub>surf</sub> > 0.15, leading to unstable direct O/W emulsions  
244 (Binks, & Lumsdon, 2000).

245

	10'	15'	30'	45'	1H	2H
<b>C8</b>	$DS_{surf} = 0.04$	$DS_{surf} = 0.07$	$DS_{surf} = 0.13$	$DS_{surf} = 0.19$	$DS_{surf} = 0.24$	$DS_{surf} = 0.38$
<b>C10</b>	$DS_{surf} = 0.06$	$DS_{surf} = 0.09$	$DS_{surf} = 0.16$	$DS_{surf} = 0.22$	$DS_{surf} = 0.26$	$DS_{surf} = 0.35$
<b>C12</b>	$DS_{surf} = 0.05$	$DS_{surf} = 0.08$	$DS_{surf} = 0.15$	$DS_{surf} = 0.20$	$DS_{surf} = 0.24$	$DS_{surf} = 0.33$
<b>C14</b>	$DS_{surf} = 0.04$	$DS_{surf} = 0.07$	$DS_{surf} = 0.14$	$DS_{surf} = 0.19$	$DS_{surf} = 0.25$	$DS_{surf} = 0.41$
<b>C16</b>	$DS_{surf} = 0.04$	$DS_{surf} = 0.07$	$DS_{surf} = 0.13$	$DS_{surf} = 0.20$	$DS_{surf} = 0.26$	$DS_{surf} = 0.52$
<b>C18</b>	$DS_{surf} = 0.05$	$DS_{surf} = 0.08$	$DS_{surf} = 0.16$	$DS_{surf} = 0.23$	$DS_{surf} = 0.30$	$DS_{surf} = 0.50$

246

247 **Fig. 5.** Pictures of the hexadecane-in-water emulsions stabilized by the CNCs modified with  
 248 long acyl chains (C8 to C18) and various  $DS_{surf}$  (obtained after 10', 15', 30', 45', 1h and 2h of  
 249 reaction), observed after 24h of storage at room temperature (W/O ratio = 80/20 v/v). The  
 250  $DS_{surf}$  estimated from the trend curves in Fig. 4 are also reported.

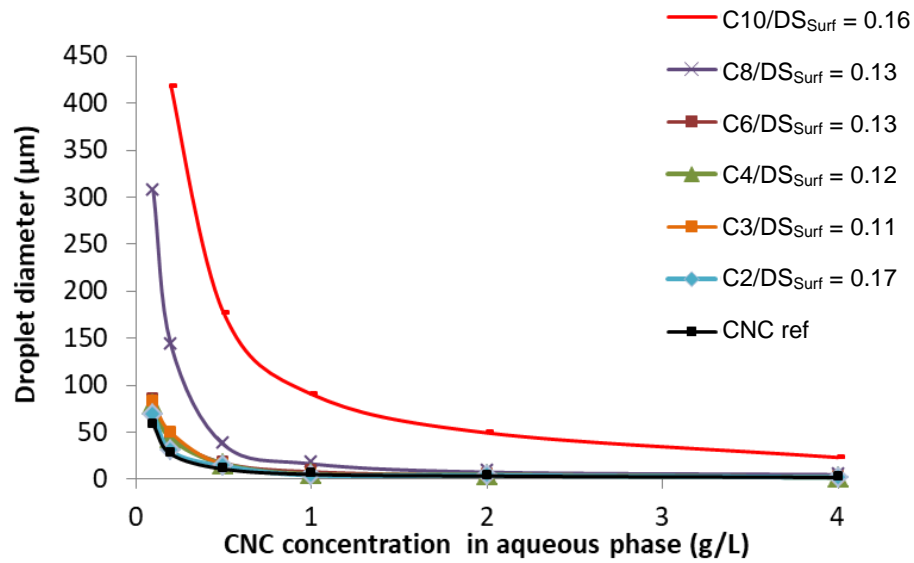
251 The CNCs concentration dependence on the average drop diameter of the direct O/W  
 252 emulsions was determined for the different CNC samples. When the concentration of native  
 253 CNCs was increased from 0.1 to 4 g/L in the aqueous phase, the droplet diameter of the  
 254 emulsion decreased until reaching a plateau at  $3\mu\text{m}$  (Fig. 6). This behavior is in accordance  
 255 with the so-called limited coalescence process (Arditty, Whitby, Binks, & Leam-Calderon,  
 256 2003). After sonication, the uncovered droplets merge; this coalescence is stopped when the

257 minimum drop coverage required for stability is reached. The drop diameter depends then  
258 directly on the amount of particle available to stabilize the interface. The second part of the  
259 curve presents a plateau. It occurs when the drop diameter cannot decrease anymore; the  
260 system will evolve at constant interface area. In many systems, the particles are released in  
261 the continuous phase but rods can move at the interface and orientate into parallel bundles  
262 leading to densification of the CNC organization (Cherhal, Cousin, & Capron, 2016). The  
263 same profile was observed in Fig. 6 for CNCs modified with short acyl chains (from C2 to  
264 C6), but differences were noted with the CNCs grafted with longer hydrophobic chains ( $\geq$   
265 C8). For these samples, a higher droplet diameter is observed at a given particles  
266 concentration and degree of substitution, as well as a shift in the concentration needed to  
267 reach the plateau at  $3\mu\text{m}$  (Fig. 6). The limited coalescence domain is controlled by the  
268 irreversible adsorption of particles at the interface. When the surface is totally covered, a  
269 plateau in drop diameter is observed. The limit concentration between these two domains was  
270 evaluated at 0.5 g/L for unmodified CNCs, 2 g/L for the CNCs grafted with C2 to C8, and  
271 more than 4 g/L for those grafted with C10. Hence, there is a clear impact of chain length on  
272 the stabilization process for direct O/W emulsions, which could result from an increasing  
273 aggregation of the CNCs at the droplets surface, through hydrophobic interactions, leading to  
274 a decrease of the total surface available for the stabilization of the O/W interface.

275 A similar result was obtained when the hydrophobicity at the surface of the particles was  
276 progressively increased with a single acyl group, through the incrementation of the  $DS_{\text{Surf}}$   
277 (Fig. 7a). To further evaluate the organization of the particles at the interface, the coverage  
278 percentage (C) for the various samples was estimated with Eq. 1, from the slope of the  
279 reciprocal surface-average diameter ( $1/D$ ) plotted as a function of CNCs concentration (for  
280 direct emulsions, and expressed in mg per ml of oil phase) (Fig. 7b). The coverage ratio  
281 decreases progressively from a fully covered surface with a value of 107 %, to a slightly



282 covered surface with a value of 27% when the  $DS_{surf}$  increased from 0 to 0.19 respectively,  
283 confirming the enhanced aggregation state of the CNCs at higher modification rate. A similar  
284 aggregation has been reported in the literature after reduction of the electrostatic repulsions  
285 between native CNCs, through desulfatation of their surface (Cherhal, Cousin, & Capron,  
286 2016), leading to a more porous and heterogeneous droplet surface.

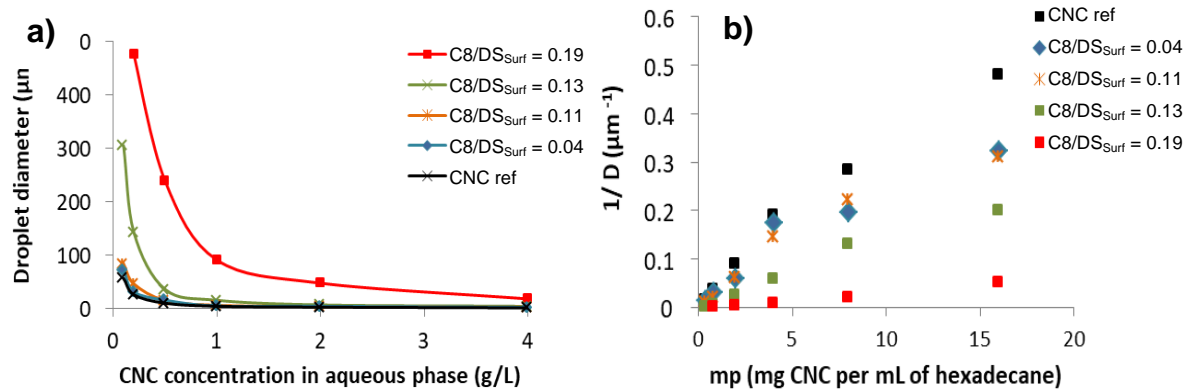


287  
288 **Fig. 6.** Evolution of the direct emulsion droplet diameter with increasing particles  
289 concentration for CNCs grafted with acyl chains of C2 to C10, with a  $DS_{surf}$  in the same order  
290 of magnitude (the  $DS_{surf}$  was estimated from the trend curves in Fig. 4).

291

292

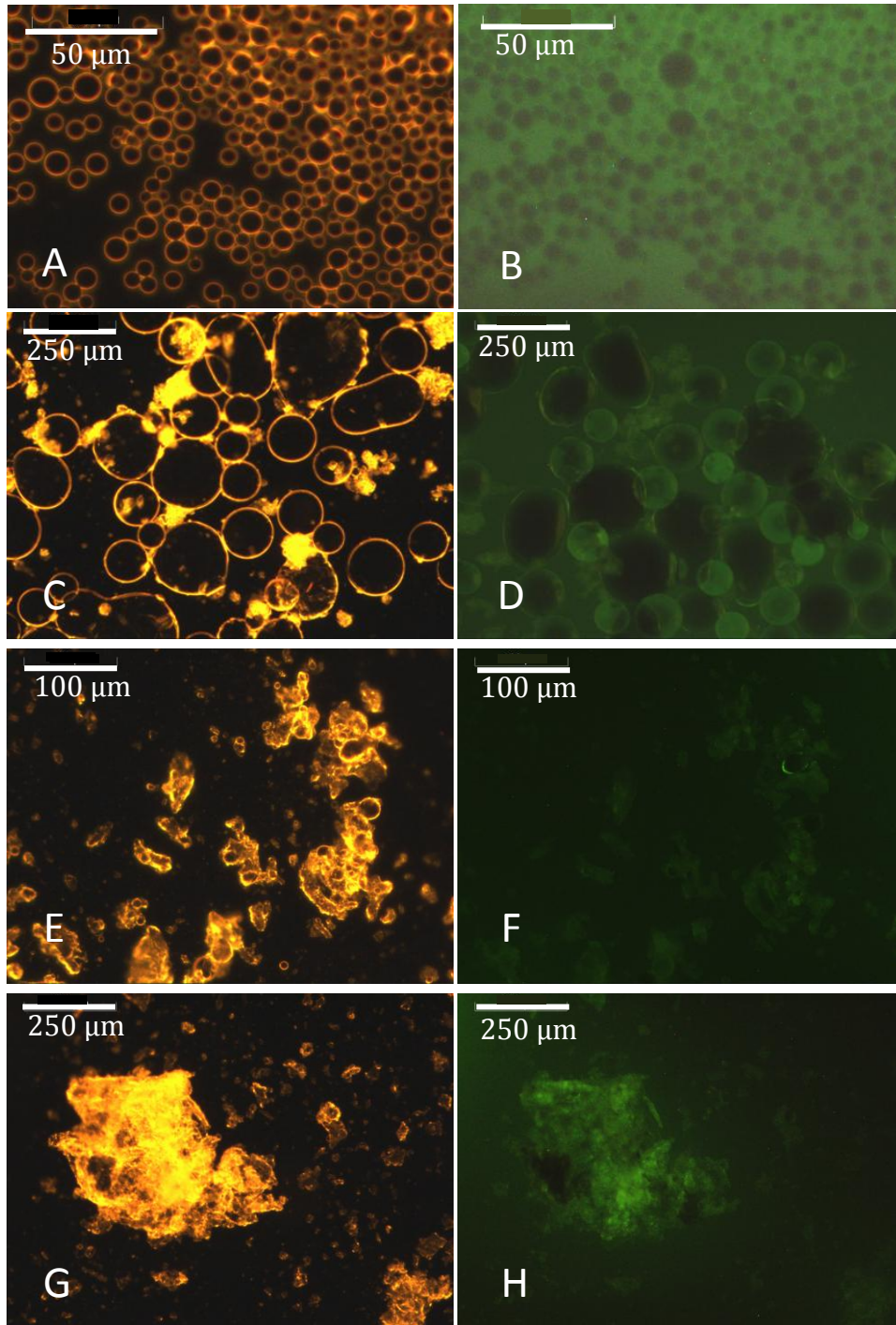
293



294  
 295 **Fig. 7. a)** Evolution of the direct emulsion droplet diameter with increasing particles  
 296 concentration for the CNCs grafted with C8 acyl chains of various DS<sub>surf</sub> (the DS<sub>surf</sub> was  
 297 estimated from the trend curves in Fig. 4). **b)** Inverse D(3,2) diameter plotted as a function of  
 298 particles concentration (expressed in mass of CNCs per mL of hexadecane).

299 All the O/W emulsions were further confirmed by staining the water continuous phase  
 300 with fluorescein (appearing in green) and visualizing the droplets with a fluorescence  
 301 microscope. Some typical results are exemplified in Fig. 8. The CNCs grafted with short acyl  
 302 chains (C2 to C6, regardless of the DS<sub>surf</sub>), or long chains and low DS<sub>surf</sub> (C8 to C18 and  
 303 DS<sub>surf</sub> ≤ 0.15), led to O/W emulsions with small oil droplets (about 3 μm) and low size  
 304 distributions in the images (Fig. 8A-B). The oil droplets that are creaming can be seen in  
 305 black in contact with the slide in Fig. 8B, while the continuous phase appears clearly in green.

306  
 307  
 308  
 309



310

311 **Fig. 8.** Optical (A, C, E, G) and fluorescence (B, D, F, H) microscopy images of a typical  
 312 (A-B) direct O/W emulsion (here: C8-graft with  $DS_{\text{surf}} = 0.13$ ), (C-D) intermediate state  
 313 where oil droplets co-exist with aggregated water droplets (here: C8-graft with  $DS_{\text{surf}} = 0.24$ ),  
 314 and (E-H) inverse W/O emulsion (here: C8-graft with  $DS_{\text{surf}} = 0.38$ ).

315

### 316 3.3 Inverse W/O emulsions

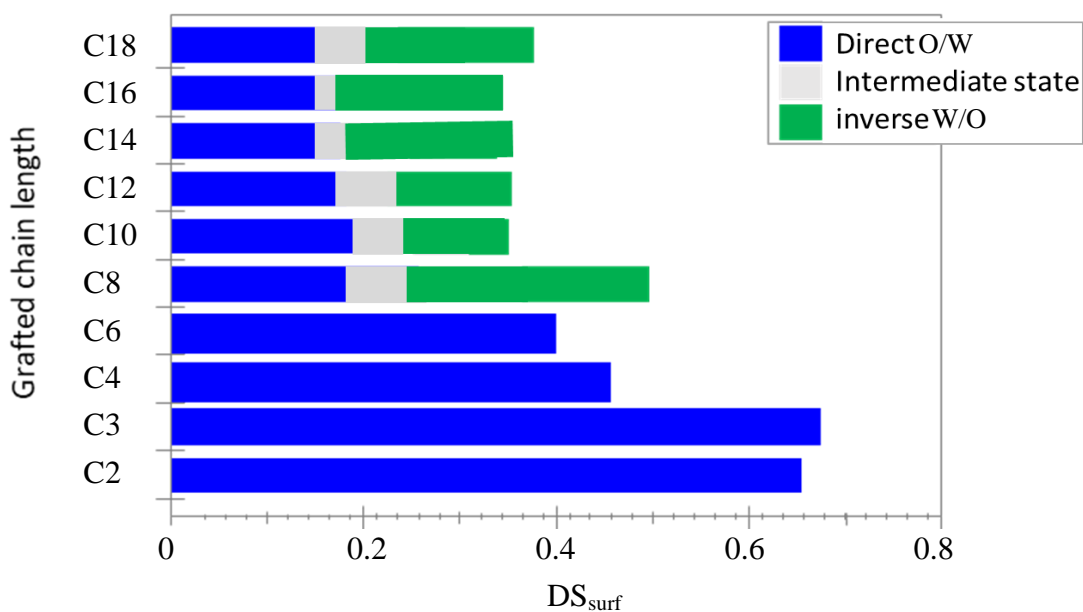
317 In a second set of experiments, emulsions were prepared by dispersing the hydrophobized  
318 CNCs in the oil phase, then sonicating the suspension with a lower volume of water (W/O =  
319 20/80 v/v), with the objective to produce inverse emulsions. Here again, the type of emulsion  
320 was inferred by observing what happens when a drop of emulsion was added to a volume of  
321 either hexadecane or water (Fig. S1 in Supplementary Material). In these conditions, only the  
322 particles grafted with acyl chains of 8 carbons or more produced inverse W/O emulsions, and  
323 only when the particles surface was sufficiently modified (i.e. when  $DS_{\text{surf}}$  was above 0.2-0.3,  
324 depending on the acyl chain). The formation of W/O emulsions with the longer acyl chains  
325 was further confirmed by fluorescence microscopy, the water encapsulated in the oil phase  
326 appearing in the form of various irregular structures that may correspond to coalesced water  
327 droplets (Fig. 8E-G and Fig. S2 in Supplementary Material). It has been indeed shown in a  
328 comprehensive study by Simovic & Prestidge 2004, that for hydrophobic nanoparticles coated  
329 droplets, the limited coalescence process can result in a flocculated network composed of  
330 coalesced droplets of irregular shapes. At intermediate  $DS_{\text{surf}}$ , the microscopy images revealed  
331 an intermediate state, where creaming oil droplets seem to co-exist with aggregated water  
332 droplets (Fig. 8C-D). These microscopic observations are quite puzzling, but could be related  
333 to the co-existence of CNCs of low and high acylation levels when the reaction time is  
334 intermediate; the initial cellulosic substrate is indeed quite variable and the calculated  $DS_{\text{surf}}$   
335 represents only an average estimate. Besides, the oil droplets observed in this intermediate  
336 state are larger than those of the direct emulsions, confirming that less low-acylated particles  
337 are available to stabilize this interface, some of the particles (the more acylated ones) being  
338 probably consumed by the interface of the water droplets seen in the microscopic images.

339 The different types of emulsions obtained in our experiments are summarized in Fig. 9, as  
340 a function of chain length (C2 to C18) and surface degree of substitution ( $DS_{\text{surf}} = 0.04$  to

341 0.69). These results show that, with the  $DS_{\text{surf}}$  obtained in our experimental conditions ( $DS_{\text{surf}}$   
342  $\leq 0,7$ ), it is never possible to produce inverse emulsions with short alkyl chains (C2 to C6). In  
343 the better case, less than 50% of the surface OH groups are substituted (the theoretical  
344 maximum  $DS_{\text{surf}}$  being 1.5), which is too low to impart a sufficient hydrophobicity to the  
345 CNCs surface and stabilize W/O emulsions with such short lengths. Distinctively, all the  
346 particles grafted with more than 8 carbons allow the stabilization of both direct and inverse  
347 emulsions, depending on the level of grafting. If O/W emulsions necessitate low  $DS_{\text{surf}}$ , the  
348 stabilization of W/O emulsions is possible only when the CNCs surface is sufficiently  
349 modified by the long chains. Beyond 8 carbons, inverse emulsions are indeed systematically  
350 produced if  $DS_{\text{surf}} > 0.25$ , i.e. when about one third of the surface OH groups are substituted.  
351 However, long chains will tend to entangle via hydrophobic interactions, leading to large  
352 particles assemblies and low surface coverage of the droplets at the interface; more material is  
353 consequently required for an efficient surface stabilization in that case. It can be noted that  
354 similar results were obtained when the hexadecane oil was replaced by toluene (results not  
355 shown).

356

357



358

359 **Fig. 9.** Type of emulsion obtained in our experimental conditions as a function of  $DS_{\text{surf}}$  and  
 360 number of carbons in the grafted chain. Direct and inverse emulsions are obtained with  $W/O$   
 361  $= 80/20$  and  $20/80$  v/v, respectively. The intermediate state corresponds to a situation where  
 362 both oil and water droplets are present in the medium according to the microscopic  
 363 observations.

#### 364 4. Conclusions

365 This work investigates the potential of surface acylation as a tool to monitor the  
366 properties of Pickering emulsions stabilized by cellulose nanocrystals (CNCs), through the  
367 control of the grafted chain length and grafting level. Amphiphilic CNCs grafted with acyl  
368 groups of various chain lengths and surface degree of substitution ( $DS_{surf}$ ) were produced,  
369 through an acylation reaction based on the transesterification of vinyl esters. The grafting was  
370 confirmed by FT-IR and  $^{13}C$  CP-MAS NMR spectroscopy, and quantified by the calculation  
371 of the surface degree of substitution ( $DS_{surf}$ ) obtained from the NMR spectra. Whatever the  
372  $DS_{surf}$ , CNCs grafted with linear acyl chains of 2 to 6 carbons led to the exclusive formation  
373 of direct O/W emulsions with hexadecane. When the linear chain contained 8 carbons or  
374 more, both O/W and W/O emulsions could be obtained at low and high  $DS_{surf}$ , respectively.  
375 The inverse W/O emulsions could be stabilized only when at least one third of the surface OH  
376 groups were substituted. At intermediate  $DS_{surf}$ , the microscopic investigations revealed the  
377 existence of an intermediate situation where both oil and water droplets seem to co-exist,  
378 which could be related to the variability of the acylation process (co-existence of CNCs of  
379 low and high acylation levels). The chain length and  $DS_{surf}$  had a clear impact on the  
380 stabilization process for direct O/W emulsions, larger droplets being obtained for a given  
381 particles concentration at higher chain length and  $DS_{surf}$ . This was assigned to an increasing  
382 aggregation of the CNCs at the droplets surface, through hydrophobic interactions, leading to  
383 a decrease of the total surface available for the stabilization of the O/W interface. As a  
384 consequence, the surface coverage of the emulsion droplets is significantly varied, which  
385 should have an impact on the permeability of the Pickering capsules in delivery applications.  
386 In any case, we were able to monitor the type of emulsion formed, droplet size and surface  
387 coverage at the oil/water interface, by adjusting the length of the grafted chain,  $DS_{surf}$ , and  
388 particles concentration.

389

## 390 **Acknowledgements**

391 This work was financially supported by INCREASE among the project BiCoM. The authors  
392 are grateful to BIBS platform. We also thank Xavier Falourd (BIBS platform INRAE-  
393 Nantes) and Céline Moreau (BIA-NANO INRAE-Nantes) for degree of substitution analysis  
394 using CP-MASS NMR.

## 395 **Supplementary material**

396 Supplementary material related to this article can be found in the online version.

## 397 **References**

- 398 Arditty, S., Whitby, C. P., Binks, B. P., Schmitt, V., & Leal-Calderon, F. (2003). Some  
399 general features of limited coalescence in solid-stabilized emulsions. *European Physical*  
400 *Journal E*, 11(3), 273-281.
- 401 Attala, R. H., Gast, J. C., Sindorf, D. W., Bartuska, V. J., & Maciel, G. E. (1980). Carbon-13  
402 NMR spectra of cellulose polymorphs. *Journal of the American Chemical Society*, 102  
403 (9), 3249-3251.
- 404 Belanger, S. E., Dorn, P. B., Toy, R., Boeije, G., Marshall, S. J., Wind, T., Van Compernelle  
405 R., & Zeller, D. (2006). Aquatic risk assessment of alcohol ethoxylates in North America  
406 and Europe. *Ecotoxicology and Environmental Safety*, 64(1), 85-99.
- 407 Binks, B. P., & Lumsdon, S. O. (2000). Influence of Particle Wettability on the Type and  
408 Stability of Surfactant-Free Emulsions. *Langmuir*, 16(23), 8622-8631
- 409 Binks, B. P. (2002). Macroporous silica from solid-stabilized emulsion templates. *Advanced*  
410 *Materials*, 14(24), 1824-1827.



411 Brand, J., Pecastaings, G., Sèbe, G. (2017). A versatile method for the surface tailoring of  
412 cellulose nanocrystal building blocks by acylation with functional vinyl esters.  
413 *Carbohydrate Polymers*, 169, 189-197.

414 Capron, I., Rojas, O. J., & Bordes, R. (2017). Behavior of nanocelluloses at interfaces.  
415 *Current opinion in colloid and interface science*, 29, 83-95.

416 Cherhal, F., Cousin, F., & Capron, I. (2016). Structural Description of the Interface of  
417 Pickering Emulsions Stabilized by Cellulose Nanocrystals. *Biomacromolecules*, 17(2),  
418 496-502.

419 Cunha, A. G., Mougel, J.-B., Cathala, B., Berglund, L. A., & Capron, I. (2014). Preparation of  
420 Double Pickering Emulsions Stabilized by Chemically Tailored Nanocelluloses.  
421 *Langmuir*, 30(31), 9327-9335.

422 Dhuiège, B., Pecastaings, G., Sèbe, G. (2019). A Sustainable approach for the Direct  
423 Functionalization of Cellulose Nanocrystals Dispersed in Water by Transesterification of  
424 Vinyl Acetate. *ACS Sustainable Chemistry & Engineering*, 7, 187-196.

425 Eyley, S., & Thielemans, W. (2014). Surface modification of cellulose nanocrystals.  
426 *Nanoscale*, 6(14), 7764-7779.

427 Goodlett, V. W., Dougherty, J. T., Patton, H. W. (1971). Characterization of cellulose acetates  
428 by nuclear magnetic resonance. *Journal of Polymer Science Part A-1: Polymer*  
429 *Chemistry*, 9, 155-161.

430 Habibi, Y. (2014). Key advances in the chemical modification of nanocelluloses. *Chem Soc*  
431 *Rev*, 43, 1519-1542.

432 Habibi, Y., Lucia, L. A., & Rojas, O. J. (2010). Cellulose Nanocrystals: Chemistry, Self-  
433 Assembly, and Applications. *Chemical Reviews*, 110(6), 3479-3500.

434 Kalashnikova, I., Bizot, H., Cathala, B., & Capron, I. (2011). New Pickering Emulsions  
435 Stabilized by Bacterial Cellulose Nanocrystals. *Langmuir*, 27(12), 7471-7479.

436 Kalashnikova, I., Bizot, H., Cathala, B., & Capron, I. (2012). Modulation of Cellulose  
437 Nanocrystals Amphiphilic Properties to Stabilize Oil/Water Interface.  
438 *Biomacromolecules*, 13(1), 267-275.

439 Lee, K.-Y., Blaker, J. J., Murakami, R., Heng, J. Y. Y., Bismarck, A. (2014). Phase Behavior  
440 of Medium and High Internal Phase Water-in-Oil Emulsions Stabilized Solely by  
441 Hydrophobized Bacterial Cellulose Nanofibrils, *Langmuir*, 30 (2), 452–460.

442 Moon, R. J., Martini, A., Nairn, J., Simonsen, J., & Youngblood, J. (2011). Cellulose  
443 nanomaterials review: structure, properties and nanocomposites. *Chemical Society*  
444 *Reviews*, 40(7), 3941-3994.

445 Pickering, S. U. (1907). Emulsions. *Journal of Chemical society* 91, 2001-2021.

446 Sèbe, G., Ham-Pichavant, F., Pecastaings, G. (2013). Dispersibility and Emulsion-Stabilizing  
447 Effect of Cellulose Nanowhiskers Esterified by Vinyl Acetate and Vinyl Cinnamate.  
448 *Biomacromolecules*, 14 (8), 2937–2944.

449 Simovitch, S., Prestidge, C. A. (2004). Nanoparticles of varying hydrophobicity at the  
450 emulsion droplet-water interface: adsorption and coalescence stability. *Langmuir*, 20,  
451 8357-8365.

452 Werner, A., Schmitt, V., Sèbe, G., Héroguez, V. (2017). Synthesis of surfactant-free micro-  
453 and nanolatexes from Pickering emulsions stabilized by acetylated cellulose nanocrystals.  
454 *Polymer Chemistry*, 17, 8 (39), 6064–6072.

455 Werner, A., Sèbe, G., Héroguez, V. (2018). A new strategy to elaborate polymer composites  
456 via Pickering emulsion polymerization of a wide range of monomers. *Polymer*  
457 *Chemistry*, 9, 5043-5050.

458 Werner, A., Schmitt, V., Sèbe, G., Héroguez, V. (2019). Convenient synthesis of hybrid  
459 polymer materials by AGET-ATRP polymerization of Pickering emulsions stabilized by  
460 cellulose nanocrystals grafted with reactive moieties. *Biomacromolecules*, 20, 490-501.

461 Xhanari, K., Syverud, K., Stenius, P. (2011). Emulsions stabilized by microfibrillated  
462 cellulose: The effect of hydrophobization, concentration and o/w ratio, *Journal of*  
463 *Dispersion Science & Technology*. 32 (3) 447– 452.

464 Zhang, Z., Tam, K. C., Wang, X., Sèbe, G. (2018). Inverse Pickering emulsions stabilized by  
465 cinnamate modified cellulose nanocrystals as templates to prepare silica colloidosomes.  
466 *ACS Sustainable Chemistry & Engineering*, 6, 2583-2590.

467

468

469

470

471

472

473

474